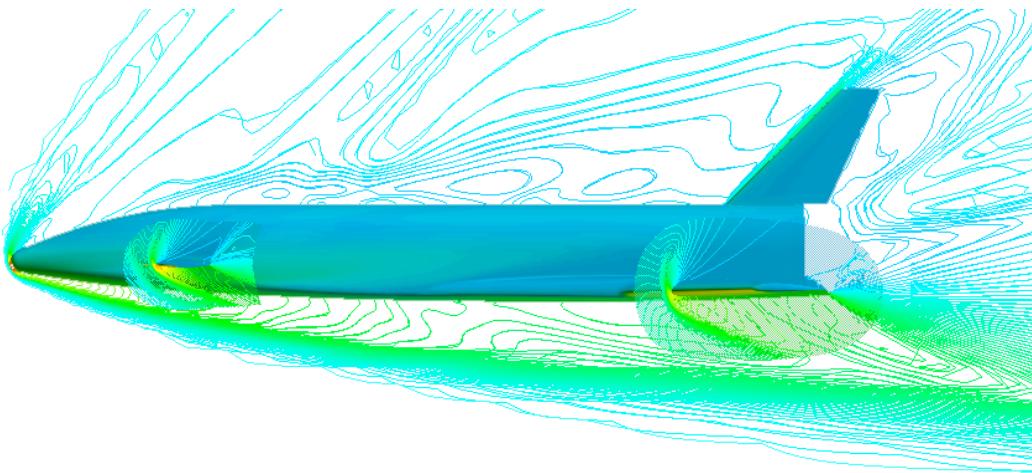




AIAA 2003-3788
Automated CFD Database Generation
for a 2nd Generation Glide-Back Booster

Neal M. Chaderjian, Stuart E. Rogers,
Michael J. Aftosmis and Shishir A. Pandya
NASA Ames Research Center
Moffett Field, California

Jasim U. Ahmad and Edward Tejnil
ELORET Institute
Moffett Field, California



21st AIAA Applied Aerodynamics Conference
23-26 June, 2003 / Orlando, Florida

Automated CFD Database Generation for a 2nd Generation Glide-Back Booster

Neal M. Chaderjian[□], Stuart E. Rogers[†], Michael J. Aftosmis[‡], Shishir A. Pandya[§]
NASA Ames Research Center, Moffett Field, California 94035

Jasim U. Ahmad[¶] and Edward Tejnil^{**}
ELORET, Moffett Field, California 94035

Abstract

A new software tool, AeroDB, is used to compute thousands of Euler and Navier-Stokes solutions for a 2nd generation glide-back booster in one week. The solution process exploits a common job-submission grid environment using 13 computers located at 4 different geographical sites. Process automation and web-based access to the database greatly reduces the user workload, removing much of the tedium and tendency for user input errors. The database consists of forces, moments, and solution files obtained by varying the Mach number, angle of attack, and sideslip angle. The forces and moments compare well with experimental data. Stability derivatives are also computed using a monotone cubic spline procedure. Flow visualization and three-dimensional surface plots are used to interpret and characterize the nature of computed flow fields.

Introduction

The past two decades have seen a sustained increase in the use of Computational Fluid Dynamics (CFD) in basic research, aircraft design, and the analysis of post-design issues. One can use a range of fidelities to model the flow field, e.g., engineering databases and panel methods to the Euler and Reynolds-averaged Navier-Stokes (RANS) equations. As the fidelity of a CFD method increases the number of cases that can be readily and affordably computed greatly diminishes. However, computer speeds now exceed 2 GHz, hundreds of processors are currently available and more affordable, and advances in parallel CFD algorithms scale more readily with large numbers of processors. All of these factors make it feasible to compute thousands of high fidelity cases. Applications that were previously thought of as unrealistic are now

possible. For example, a sizeable CFD database can be used by itself or in combination with other databases to evaluate an aircraft's stability derivatives, or explore its handling qualities in a flight simulator with a pilot-in-loop.

Even when one is able to generate many solutions, there are other practical issues. How does one execute, monitor, and post-process thousands of cases? Software is needed to reduce the tedious nature of the problem, personnel workload, and tendency for human error that can easily overwhelm a team of engineers. One example of process automation is the ILab software.¹ This software provides a general purpose capability for creating and launching parameter studies. Due to its generality, significant user input is needed to customize it for a particular application. Chaderjian et al.² is another example of process automation. In this example, PERL scripts and a PERL Graphical User Interface (GUI) were used to generate a database of solutions and post-process the results for a Harrier in ground effect using a time-dependent RANS method. These scripts greatly reduced the user workload, but used only one CFD code and one geographical site.

A major focus of the Computing, Networking, and Information Systems (CNIS) Project, which is part of the NASA Computing, Information and Communication Technologies (CICT) Program is to facilitate the use of distributed heterogeneous computer systems (grid computing)³ for generating large numbers of CFD solutions. Grid computing is based on the concept that one could gain significant increases in computational throughput by accessing any number of remote computer nodes through a common job-submission mechanism. The Globus⁴ software provides a common job-submission mechanism, secure services for user authentication, remote shell execution, and secure file transfers over an open network.

The objective of the current work is to build and demonstrate a prototype software system (AeroDB) that is based on Globus and will automate the process of running CFD jobs on grid resources. This software is used to meet a CNIS milestone of generating at least 100 RANS solutions and 1000 Euler solutions in one week for a 2nd generation Langley Glide-Back Booster (LGBB) design. A companion paper by Rogers et al.⁵

[□] Research Scientist, Associate Fellow AIAA.

[†] Aerospace Engineer, Associate Fellow AIAA.

[‡] Research Scientist, Senior Member AIAA.

[§] Research Scientist, Member AIAA.

[¶] Senior Research Scientist.

^{**} Research Scientist.

This paper is a work of the U.S. Government and is not subject to copyright protection in the United States.

describes in detail the AeroDB software. This paper focuses on presenting the results for the LGBB geometry.

The solution procedure is described in the next section, including a brief overview of the AeroDB framework, a description of the LGBB geometry, and the CFD codes used to generate a parametric database. The results are then presented, including validation of the computations with wind-tunnel data, visualization of the computed flows, and the effects of flow conditions on the computed forces and moments. Concluding remarks are then given.

Solution Procedure

A solution procedure for computing a database of Euler and RANS solutions for a LGBB geometry is now described.

AeroDB

AeroDB is a system of PERL scripts and a MySQL⁶ database. The solution process begins with a job-submission script. This script enters the matrix of cases to be run by a particular user into the database. In the present case, the Mach number, angle of attack, and sideslip angle are varied. Other parameters, such as the flow solver, number of CPUs per case, etc. are also specified in the script. A job-launcher script is continually running in the background and checks the database for new cases to run, or continuing jobs that need multiple submissions (restarts) for completion. This script also utilizes a resource discovery algorithm to decide where to submit the jobs. The cases are allocated to different sites and computers depending of the current workload for each machine. For the present application, 13 computers at 4 different geographical sites across the United States are used.

Once a job begins to execute at a remote site, a Remote Execution Script (RES) manages the run. It handles data transfers between the execution computer and a mass storage system. It also monitors the run, frequently checking how much remaining time is left, and whether or not a solution is converged or needs to be resubmitted for additional runs. The user does not need to specify how long to run the job, or how many iterations to execute in a particular run queue. The RES utilizes a Run-Manager (RM) library for monitoring flow-solver progress. The RM library is called from the flow solver.

Finally, a web portal can be used by the user to check on the status of each job in the database. The user can also use the web portal to stop, cancel, restart, modify, delete, or re-run jobs. The web portal is password protected and can be used anywhere internet

access is available. The user controls and monitors computer jobs only through the job-submission script and the web portal. AeroDB automatically handles everything else. Additional details of AeroDB can be found in Rogers et al.⁵

LGBB Geometry

The LGBB geometry shown in Fig. 1 is a 2nd generation glide-back booster concept developed at NASA Langley Research center as part of the NASA Space Launch Initiative (SLI) Program. This geometry is used in the present computations, which includes the fuselage, wings, Leading Edge Extensions (LEX), canards, and vertical tail. A full-body geometry is used in all computations, including zero sideslip cases. The wing's elevons and vehicle's exhaust nozzle are not included, but can be added in the future.

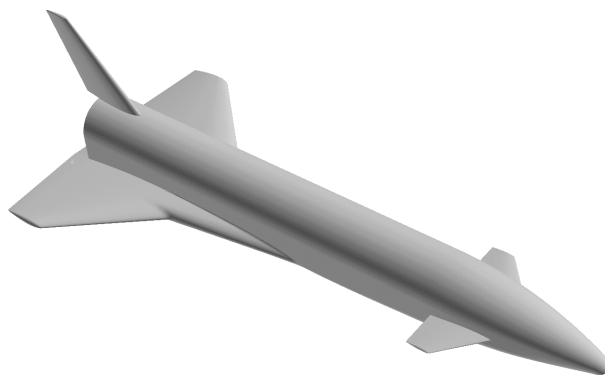


Fig. 1 Langley glide-back booster geometry.

Euler Flow Solver

The Cart3D Euler code^{7,8} is used to compute inviscid flows with unstructured Cartesian meshes. Cart3D is an automated and robust grid generation and flow solver package. An example of a Cartesian grid system generated for the LGBB geometry with wind-tunnel sting is shown in Fig. 2. The only data required to generate this grid is a triangulated surface geometry. The code then generates an unstructured Cartesian mesh with automated grid refinement based on the geometry and pre-specified regions of refinement. This results in highly refined cells near regions of high surface curvature and coarser cells away from the body. The intersection of the solid geometry with the regular Cartesian hexahedra is computed, and polyhedral cells are formed which contain the solid surface at one end of the cell. Cells interior to the geometry are automatically removed. The solid-wall inviscid boundary conditions are then specified on these “cut-cell” polyhedra.

The grid generation procedure⁷ is robust, and does not require user intervention. The grid generation

process is also fast (over 1 million cells per minute). Because the grid generation process is fast and robust, grids are usually created on-demand in the run script on the remote host rather than stored on the mass storage system, thus reducing network transfer time. The Cart3D subsonic grids consist of about 1.4 million cells, and the supersonic grids consist of about 0.8 millions cells. Solution convergence is typically obtained in 200-300 cycles, depending on the flow conditions.

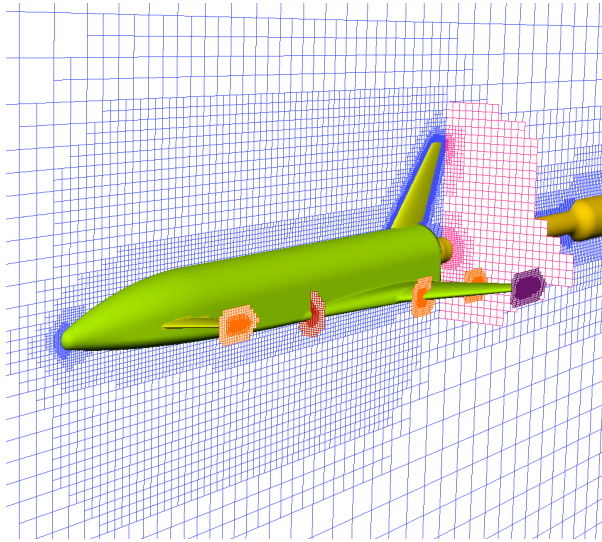


Fig. 2 Cart3D Cartesian grid system.

The flow-solver algorithm is based on an explicit multi-stage procedure with strong multigrid acceleration.⁸ Cart3D has been parallelized to efficiently run on shared-memory computers using standard OpenMP directives, and has demonstrated parallel speedups of 496 on 512 processors.

Navier-Stokes Flow Solver

The steady RANS equations are solved with the Overflow^{9,10} code, which uses overset structured grids to model complex geometries. Figure 3 shows the overset surface grids for the LGBB geometry. The volume grid system consists of 34 zones. Outer box grids are used to extend the viscous body grids to the far field. These box grids are solved with the Euler equations. The subsonic grid system has far-field boundaries located 10 body lengths from the vehicle in all three coordinate directions, and consists of over 8.5 million grid points. The supersonic grid system has its far-field boundaries located closer to the vehicle (about 1 body length away). This does not affect the solution accuracy due to domain-of-influence effects, and reduces the computational cost because of the smaller outer box grids. The grid system was generated by using an automated script system using the Chimera Grid Tools^{11,12} software and the Pegasus¹³ overset grid-joining program.

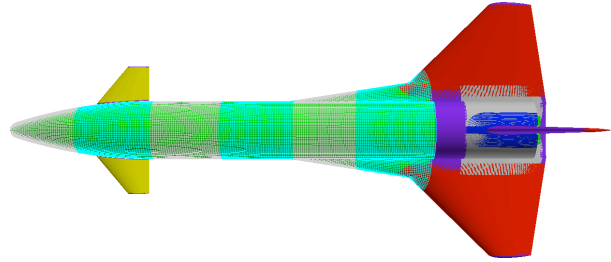


Fig. 3 Planform view of overset surface grid system.

Within the Overflow code, the implicit, approximate-factorization, diagonal algorithm due to Pulliam and Chaussee¹⁴ is used to solve the steady RANS equations with central differencing, together with the Spalart-Allmaras¹⁵ turbulence model. This algorithm was selected because of its computational efficiency. The Overflow solution procedure starts from impulsive conditions using large values of scalar dissipation, and is run for 800 steps using full multi-grid sequencing on three levels. The computation is then run to steady-state convergence using matrix dissipation and three-level multi-grid acceleration. The matrix dissipation provides lower levels of spatial damping while maintaining code stability. The matrix dissipation values suggested by Olsen and Prabhu¹⁶ were used in the present computations. The AeroDB software automates this entire run process.

Two different parallel versions of the Overflow code are used in the solution process. On distributed memory machines, a Message-Passing Interface¹⁷ (MPI) version of Overflow is used. This version of the code explicitly passes inter-zonal boundary condition data between zones as a message between the CPU's using the MPI standard. Load balancing is obtained by distributing the zones among all the CPU's. Since the zones can be significantly different in size, a CPU may be given just one zone, or multiple zones, or just part of a zone.

Improved scalability is obtained on single-image computers, e.g. NASA's SGI Origin 2000 and 3000 machines, using multi-level parallelization (MLP). Overflow-MLP¹⁸ utilizes both fine-grain (do loops) and coarse-grain (domain decomposition) approaches to improve parallel performance. Domain decomposition groups together several zones and assigns several processors to each group. The user simply selects the number of groups and processors, and the domain decomposition algorithm in the code decides how many processors to allocate to each group. It seeks to distribute the workload evenly among the available processors by taking into account the number of grid points in each group, and the fidelities assigned to each zone, i.e. Euler, thin-layer, or full Navier-Stokes equations.

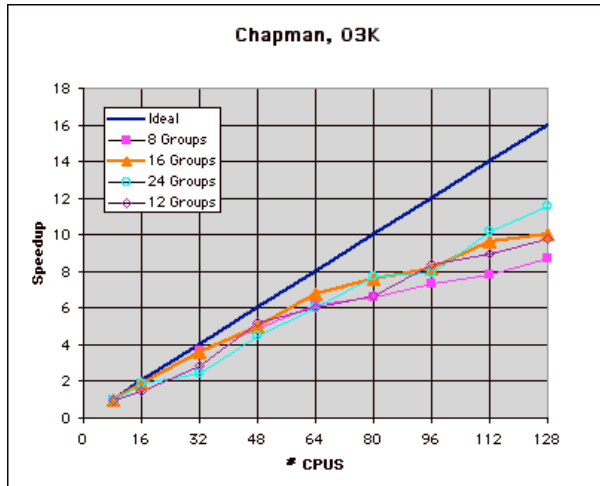


Fig. 4 Overflow-MLP scalability on an SGI Origin 3000 computer.

A scalability study for the 34 zone, 8.5 million grid point LGBB overset-grid system is shown in Fig. 4. The blue line represents ideal linear scaling based on the performance using 8 CPUs. Table 1 quantifies the parallel efficiency displayed in Fig. 4. An acceptable 84% efficiency is obtained with 64 CPUs, and 72% efficiency with 128 CPUs. The MLP approach tends to provide better scalability than the MPI approach. The scalability improves with increased grid size or number of zones.² In order to not overwhelm the available computational platforms, which are shared with other users, 8 groups and 32 CPUs were selected for running viscous cases on single-image machines. This selection has a parallel efficiency of 92%.

Table 1 Parallel Efficiency using Overflow-MLP

Number of Groups	24	8	8	12	16	24	12	24	24
Number of CPU's	8	16	32	48	64	80	96	112	128
Parallel Efficiency (%)	100	95	92	86	84	77	70	72	72

Figure 5 shows typical convergence histories of the lift coefficient C_L , drag coefficient C_D , and pitching moment C_m with iteration for subsonic cases. The change reflected at 800 steps is due to the startup process where the dissipation is switched from scalar to matrix dissipation. Supersonic cases show a similar convergence history.

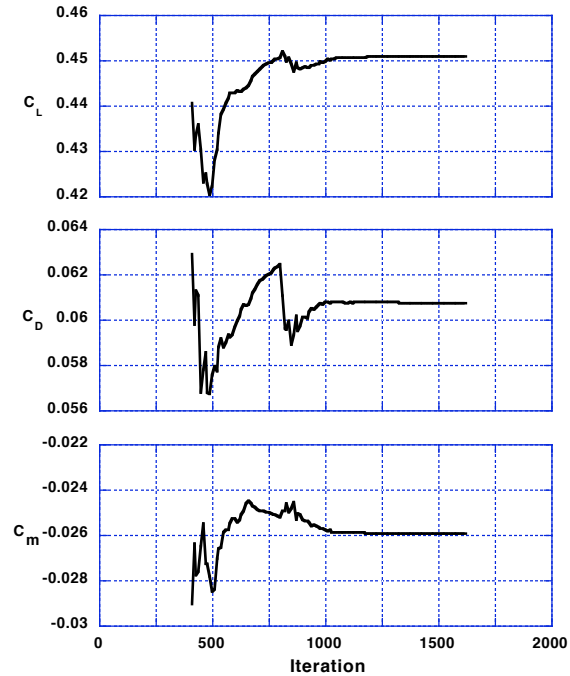


Fig. 5 Typical Overflow convergence history.

Results

AeroDB is used to generate a database of Euler and Navier-Stokes solutions for the LGBB geometry. Inviscid (Cart3D) computations were carried out using 38 Mach numbers ranging from 0.2 to 6.0, five sideslip angles ranging from 0 to 4 degrees, and angles of attack ranging from -5 to 30 degrees. Navier-Stokes (Overflow) computations were also carried out using 14 Mach numbers ranging from 0.2 to 3.0, and five sideslip angles ranging from 0 to 4 degrees. The angles of attack for the viscous cases ranged from 0 to 20 degrees for subsonic flows, and 0 to 30 degrees for supersonic flows. The supersonic viscous cases were computed with a zero sideslip angle using the automated PERL script system described by Chaderjian et al.² This was done as part of this CNIS effort, prior to the completion of AeroDB. All of the solutions are reported in this paper.

The CNIS milestone of computing at least 100 Overflow cases and 1000 Cart3D cases in one week was fully met within a 72 hour time period using AeroDB. At the end of seven days, 211 Overflow cases and 2863 Cart3D cases were completed. The current LGBB CFD database consists of 3666 cases, (499 Overflow solutions and 3167 Cart3D solutions).

Validation

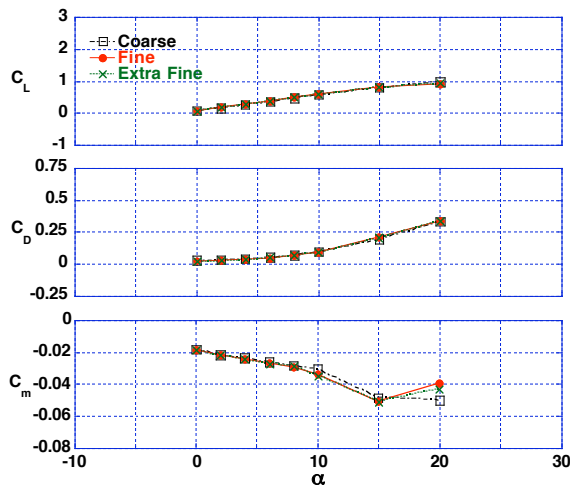
The CFD database is validated through a grid refinement study and comparison of the computed results with wind tunnel data. Due to the large size of

the database, representative cases are chosen to validate the computed results. The Overflow Navier-Stokes solutions are computed at full flight Reynolds number (Re) conditions, according to a flight trajectory scenario. This Reynolds number is based on the fuselage length.

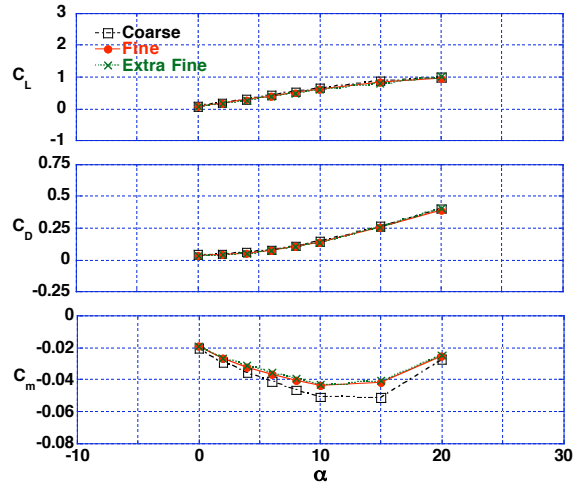
An Overflow grid refinement study is carried out using three different grids for compressible subsonic and transonic flow conditions. A coarse grid consists of about 2 million grid points. A fine grid consists of about 8.5 million grid points and has twice the resolution of the coarse grid in the two body-surface directions. An extra-fine grid consists of about 16 million grid points and has twice the resolution of the fine grid in the two body-surface directions.

Figure 6a compares the Overflow lift, drag, and pitching moment coefficients computed on all three grids with $M=0.6$. All three grids show virtually identical lift and drag coefficients up to 20 degrees angle of attack. The pitching moment coefficients compare very well with each other using the fine and extra fine grids; however, the coarse grid shows some differences when the angle of attack is above 8 degrees.

In a similar manner, Fig. 6b compares the Overflow lift, drag, and pitching moment coefficients for all three grids under transonic conditions ($M=0.9$). Once again, the computed lift and drag coefficients compare very well with each other on all three grids. The pitching moment coefficients for the fine and extra-fine grids also compare very well with each other; however, the coarse grid pitching moment coefficients are markedly different and consistently under-predict the values computed on the fine and extra-fine grids. Overall, the fine grid has adequate grid support and is used for computing the present database.



(a) $M=0.6$, $Re=115$ million.



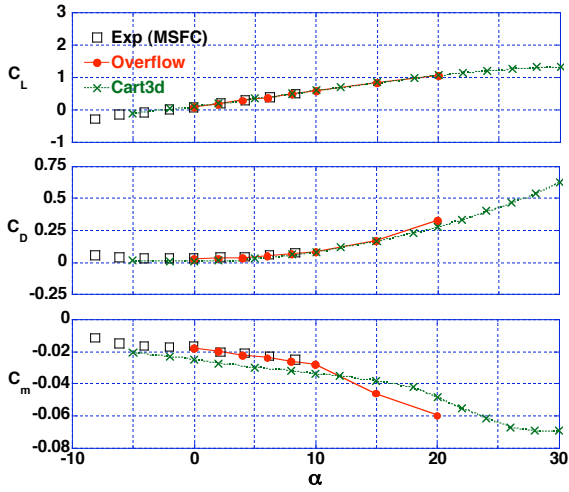
(b) $M=0.9$, $Re=60$ million.

Fig. 6 Comparison of Overflow lift, drag, and pitching moment coefficients using three different grid systems.

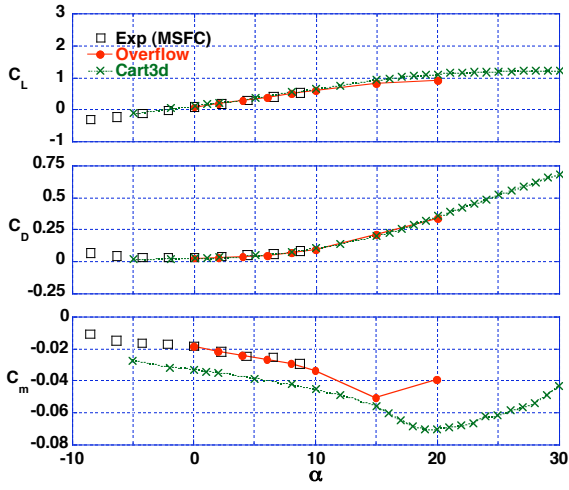
The inviscid Cart3D code^{7, 8} utilizes an advanced Cartesian grid generation algorithm with automated grid refinement as described in the Euler Flow Solver section. This procedure has been applied to a wide variety of vehicles and flow conditions, and its automated grid-refinement algorithm is used to obtain proper grid support for the present database computations.

Both Euler and Navier-Stokes solutions are compared with subsonic data that is available from NASA Marshall Space Flight Center¹⁹ for angles of attack up to 10 degrees, and zero sideslip. Supersonic data is available from NASA Langley Research Center¹⁹ for angles of attack up to 30 degrees, and zero sideslip.

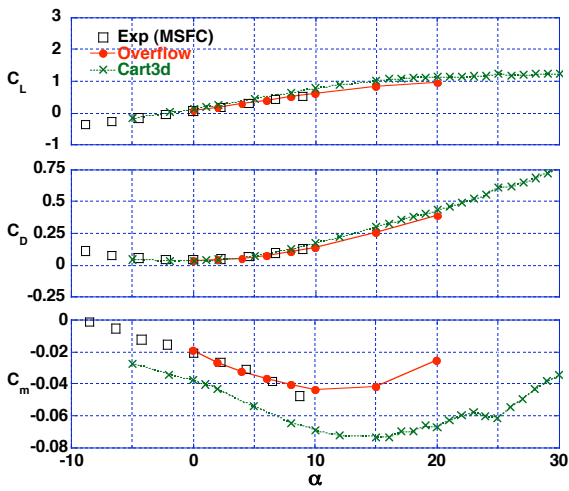
Figure 7 compares computed lift, drag, and pitching moment coefficients with wind tunnel data for several subsonic flow conditions. The Overflow lift, drag and pitching moment coefficients compare very well with the experiment. The Cart3D lift and drag coefficients compare equally well with the experiment, but under predict the pitching moment somewhat. Cart3D computations with and without a sting (not shown here) indicate the sting has very little effect on the computed forces and moments. So the differences in moment coefficients are attributed to viscous effects. Overall, the subsonic computed results compare well with the experimental data.



(a) $M=0.3$, $Re=98$ million.



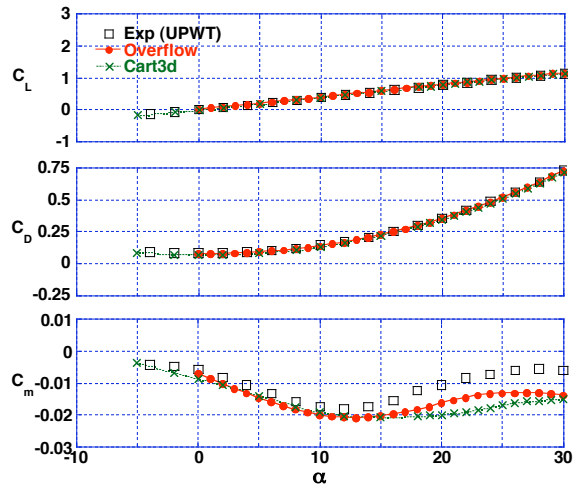
(b) $M=0.6$, $Re=115$ million.



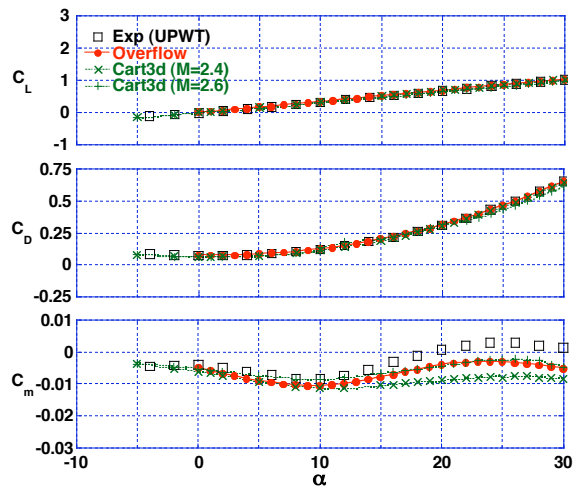
(c) $M=0.9$, $Re=60$ million.

Fig. 7 Comparison of computed lift, drag, and pitching moments with subsonic wind tunnel data.

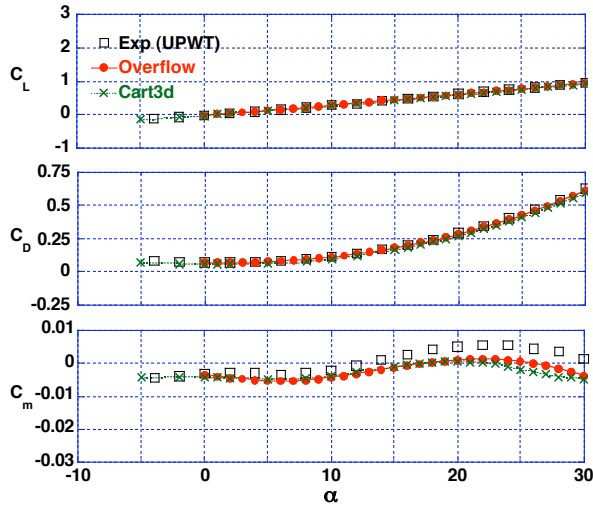
Figure 8 compares computed lift, drag, and pitching moment coefficients with wind-tunnel data for supersonic flow conditions. The Overflow and Cart3D lift and drag coefficients compare very well with the experiment. There are some minor differences between the computed and experimental pitching moment coefficients. The Overflow C_m consistently under predict the experimental values at the higher angles of attack and capture the variation of C_m with angle of attack (curve shape) very well. The Cart3D C_m also under predict the experimental values, and follow the experimental curve shape reasonably well. The Overflow C_m compare more favorably with experiment than the Cart3D values at higher angles of attack. This is probably due to viscous effects that are shown in the Visualization section. Overall, the supersonic computed results compare well with the experimental data.



(a) $M=2.0$, $Re=91$ million.



(b) $M=2.5$, $Re=88$ million.



(c) $M=3.0$, $Re=32$ million.

Fig. 8 Comparison of computed lift, drag, and pitching moments with supersonic wind tunnel data.

Visualization

Visualization of two of the viscous cases are now presented. Figure 9 shows the Overflow pressure coefficient (C_p) contours at the symmetry plane and on the surface of the LGBB, for $M=1.6$, $\alpha=20^\circ$, and $Re=75$ million. Shocks near the vehicle nose, along the vertical tail, and the aft-body region are evident. Influence of the canard shock can also be observed at the flow symmetry plane. The C_p contours at the tail end of the fuselage indicate separated flow.

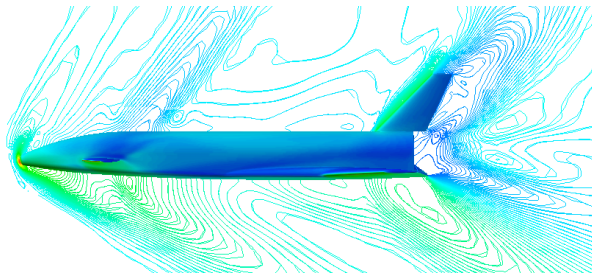


Fig. 9 Pressure coefficient contours (blue \square low C_p , green \square higher C_p). $M=1.6$, $\alpha=20^\circ$, $Re=75$ million.

Figure 10 shows the surface flow topology on the aft portion of the LGBB, and the LEX vortex (shown in red). The LEX vortex provides additional lift at the higher angles of attack. The wing surface flow indicates separated flow. However, due to domain-of-influence (DOI) effects, these separated regions are confined to very close to the body. This helps explain why there are very little viscous effects shown in the previous section for the supersonic Euler and Navier-Stokes lift and drag coefficients, but more significant effects for the pitching moments. This also explains why the flows were mostly found to be steady.

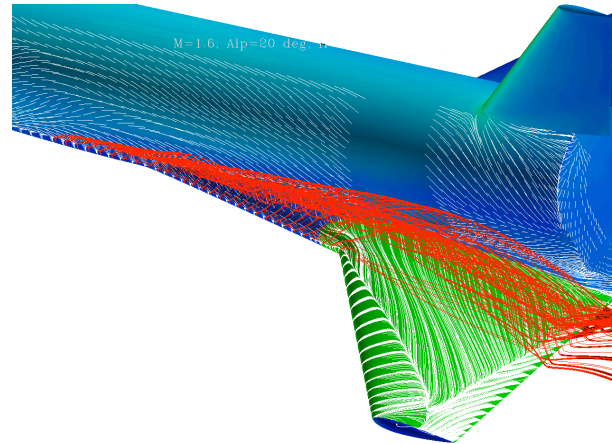


Fig. 10 Surface pressure coefficients, surface flow topology (white), and the off-surface LEX vortex (red). Wing colored green to highlight surface flow. $M=1.6$, $\alpha=20^\circ$, $Re=75$ million.

Figure 11 shows the Overflow pressure coefficient contours at the symmetry plane and on the surface of the LGBB, for $M=3.0$, $\alpha=30^\circ$, and $Re=32$ million. The shock structures are similar to those shown in Fig. 9. However, the nose shock is closer to the underside of the vehicle due to the higher Mach number and angle of attack. Cutting planes through the canard and wing sections also reveal leading and trailing edge shocks. The C_p contours at the tail end of the fuselage also indicate separated flow.

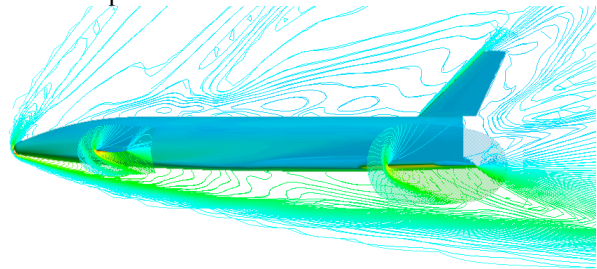


Fig. 11 Pressure coefficient contours (blue \square low C_p , green \square higher C_p). $M=3.0$, $\alpha=30^\circ$, $Re=32$ million.

Figure 12 shows the LGBB viscous surface pressure coefficient, surface flow topology, and off-surface vortical flows highlighted by helicity-density contours (yellow). It is remarkable how complex the surface-flow topology is; and as was the case in Fig. 10, the separated regions are confined to regions very close to the body and wing. This is not the case, however, for the fuselage vortex shown in yellow. The separation and reattachment lines follow the topological rules for physical flows. Primary and secondary separation and reattachment lines are also evident underneath the canard, indicating the matrix dissipation is sufficiently low so as not to wash out these flow structures.

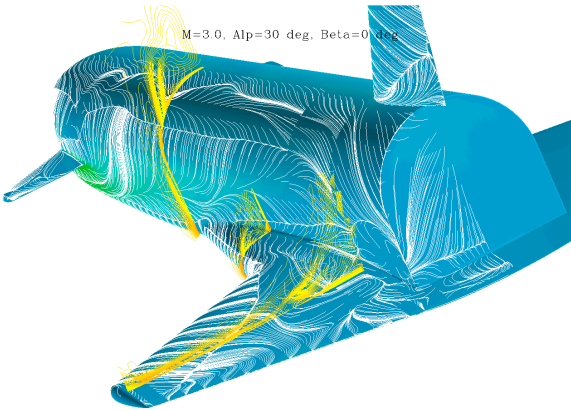


Fig. 12 Surface pressure coefficients, surface flow topology (white), and the off-surface helicity-density contours (yellow). $M=3.0$, $\alpha=30^\circ$, $Re=32$ million.

The Overflow supersonic flows can be characterized as steady, but exhibit significant flow separation at the higher angles of attack. The effects of these separated flows are minimized due to the DOI effects. The Cart3D Euler computations (not shown here) do not exhibit separated flow, as expected.

Parameter Effects

Figures 13-15 show the variation of lift, drag, and pitching moment coefficients with Mach number and angle of attack, as computed by Overflow. Symbols indicate computed cases and lines represent values obtained by using a monotone cubic-spline interpolation procedure.²⁰ The lift and drag coefficients show a trend of increasing lift and drag with angle of attack. They also exhibit a compressibility rise in the transonic region, a local ridge near $M=1$, and drop off in the supersonic region. The pitching moment coefficient shows a relatively flat behavior in the supersonic region due to shock positions being fixed near wing/canard trailing edges, and a dramatic valley in the transonic region. Here, the shock position plays an important role in determining the shape of this valley.

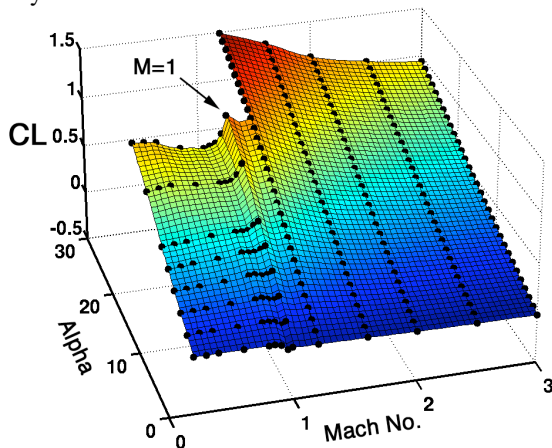


Fig. 13 Overflow lift coefficient.

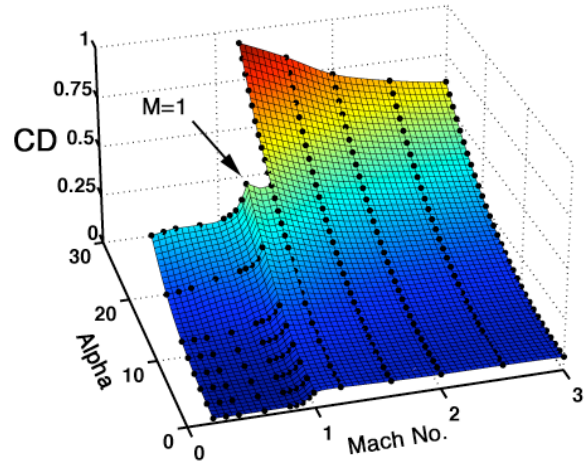


Fig. 14 Overflow drag coefficient.

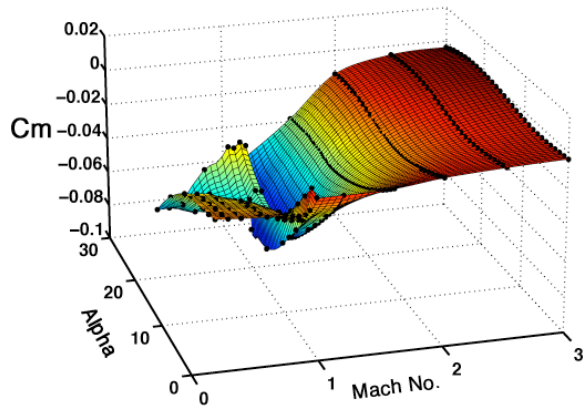


Fig. 15 Overflow pitching moment coefficient.

Figures 16-18 show the variation of the stability derivatives, $C_{L\alpha} = \partial C_L / \partial \alpha$, $C_{D\alpha} = \partial C_D / \partial \alpha$, and $C_{m\alpha} = \partial C_m / \partial \alpha$, with Mach number and angle of attack. These surfaces were generated by numerically differentiating the lift, drag, and pitching moment coefficients, using the monotone procedure reported by Butland and Fritsch.²⁰ These surfaces are useful in evaluating the stability and handling qualities of the LGBB. The lift-curve slope is seen to be higher near $M=1$, and drops off at higher angles of attack in the transonic region. The pitching-moment slope is also seen to rise near $M=1$, and is relatively flat in the supersonic region. These surfaces exhibit the same trends discussed in Figs. 13-15, but provide a different point of view of the computed data. Even when large amounts of data are available, e.g., CFD, wind-tunnel tests, or full-scale flight measurements, numerically differentiating the data can introduce very “noisy” results. Using a monotone procedure helps control this effect and provides reasonable slope information. The ability to compute thousands of cases using the AeroDB framework also provides an opportunity to “fly” the

vehicle in a virtual flight simulator before a full-sized flight vehicle is built.

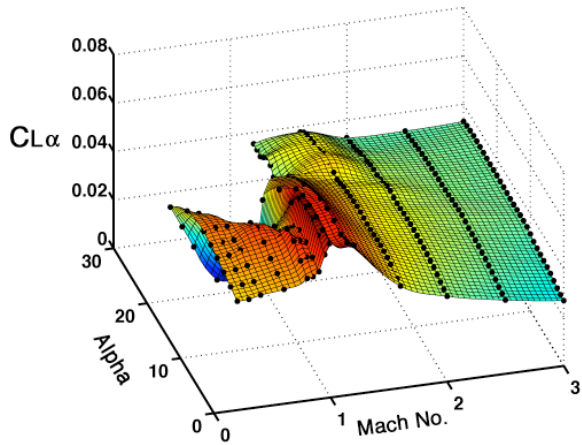


Fig. 16 Overflow lift coefficient stability derivative.

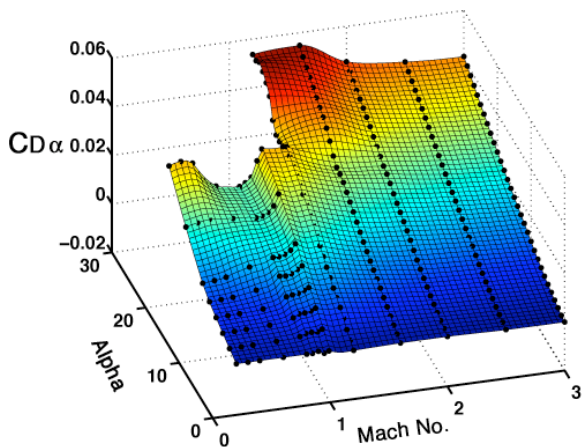


Fig. 17 Overflow drag coefficient stability derivative.

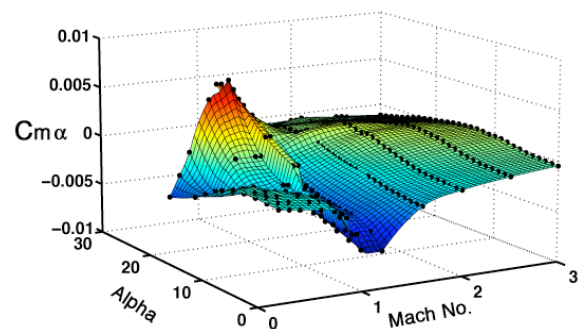


Fig. 18 Overflow pitching moment coefficient stability derivative.

Figures 19-21 show the Cart3D (inviscid) variation of lift, drag, and pitching moment with Mach number and angle of attack. These figures show the same

trends as the viscous cases (i.e., Figs. 13-15), but also provide a larger view of the parameter space. The angle of attack range is extended from -5 degrees to 30 degrees for all Mach numbers, and the Mach number range is extended up to $M=6$. The inviscid and viscous solutions differ primarily in the transonic pitching moment coefficients.

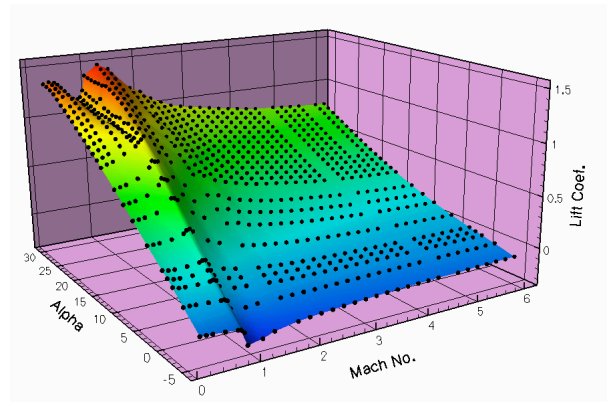


Fig. 19 Inviscid Cart3D lift coefficient.

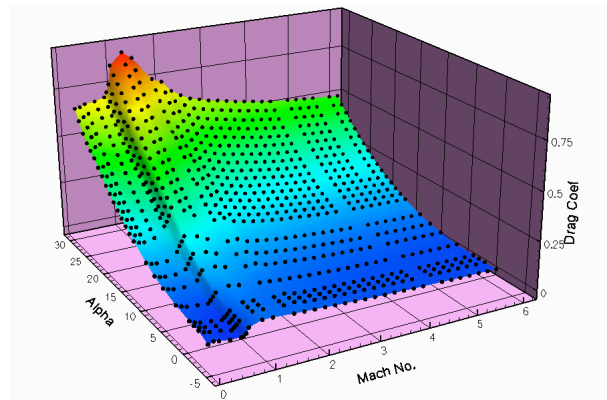


Fig. 20 Inviscid Cart3D drag coefficient.

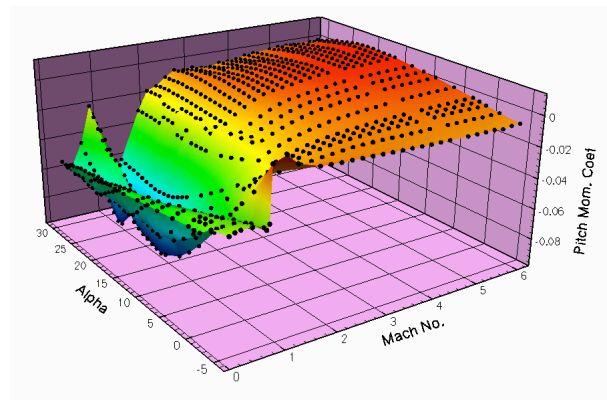


Fig. 21 Inviscid Cart3D pitching moment coefficient.

Conclusions

The ability to automate and manage the solution process for generating thousands of high fidelity CFD solutions has been demonstrated. These computations were carried out using a new software tool, AeroDB, which uses PERL scripts and a MySQL database. AeroDB utilized a grid environment to carry out these flow computations using 13 computers at 4 different geographical sites. Viscous computations were carried out with the Overflow overset grid code, and inviscid computations used the Cart3D Cartesian mesh code.

The primary goal of computing at least 100 Navier-Stokes solutions and 1000 Euler solutions for a LGGB geometry in one week was fully met in 72 hours. At the end of seven days, 211 viscous cases and 2863 inviscid cases were completed. The current LGGB CFD database consists of 3666 cases, (499 viscous and 3167 inviscid).

The computed database has a Mach number range of 0.2 to 6.0, a sideslip range of 0 to 4 degrees, and an angle of attack range of -5 to 30 degrees. Computed lift, drag, and pitching moments compared well with wind tunnel data for both subsonic and supersonic Mach numbers. The viscous supersonic flows can be characterized as steady, but exhibiting significant flow separation at the higher angles of attack. However, due to domain-of-influence effects, these separated flows were confined to regions very close to the body, and had a minimal impact on the lift and drag coefficients. The subsonic and supersonic viscous pitching moment coefficients were found to agree more closely with the experimental values than the inviscid pitching moment coefficient, indicating there are some viscous effects.

The stability derivatives ($C_{L\alpha}$, $C_{D\alpha}$, and $C_{m\alpha}$) were computed using a monotone differentiation procedure. The ability to generate thousands of CFD solutions, including their stability derivatives, provides a new opportunity to utilize CFD to explore the stability and handling qualities of new aerospace designs through direct analysis and virtual flight simulators.

Acknowledgements

The authors wish to thank Dr. Bandu N. Pamadi of NASA Langley Research Center for supplying the LGGB geometry and experimental data, and to Dr. Reynaldo Gomez of NASA Johnson Space Center for supplying some of the LGGB surface grids used in this work.

In Memoriam

This paper is dedicated to the memory of Astronaut Kalpana Chawla, who was lost on STS-107. Several of

us had the privilege of working with her as she developed and applied CFD methods to powered-lift vehicles at NASA Ames Research Center. She will be missed.

References

¹Yarrow, M., McCann, K. M., DeVivo, A., and Tejnil, E., "Production-Level Distributed Parametric Study Capabilities for the Grid," NAS Technical Report NAS-01-009, NASA Ames Research Center, 2001.

²Chaderjian, N. M., Pandya, S. A., Ahmad, J. U., and Murman, S. M., "Progress Toward Generation of a Navier-Stokes Database for a Harrier in Ground Effect," AIAA Paper 2002-5966, November 2002.

³Foster, I., "The Grid: A New Infrastructure for 21st Century Science," *Physics Today*, Vol. 55, No. 2, pp. 42-47, 2002.

⁴Foster, I., and Kesselman, C., "Globus: A Metacomputing Infrastructure Toolkit," *Int. J. Supercomputer Applications*, Vol. 11, No. 2, pp. 115-128, 1997.

⁵Rogers, S. E., Aftosmis, M. J., Pandya, S. A., Chaderjian, N. M., Tejnil, E., and Ahmad, J. U., "Automated CFD Parameter Studies on Distributed Parallel Computers," AIAA Paper 2003-4229, June 2003.

⁶Reese, G., Yarger, J. R., and King, T., Managing and Using MySQL, O'Reilly & Associates, Inc., 2nd Edition, April 2002.

⁷Aftosmis, M. J., Berger, M. J., and Melton, J. E., "Robust and Efficient Cartesian Mesh Generation for Component-Based Geometry," AIAA Paper 97-0196, Jan. 1997; *AIAA Journal*, Vol. 36, No. 6, pp. 952-960, June 1998.

⁸Aftosmis, M. J., Berger, M. J., and Adomavicius, G., "A Parallel Multilevel Method for Adaptively Refined Cartesian Grids with Embedded Boundaries," AIAA Paper 2000-0808, January 2000.

⁹Buning, P. G., Jespersen, D. C., Pulliam, T. H., Chan, W. M., Slotnick, J. P., Krist, S. E., and Renze, K. J., "Overflow User's Manual, Version 1.8t" NASA Langley Research Center, Hampton, VA, 2002.

¹⁰Jespersen, D. C., Pulliam, T. H., and Buning, P. G., "Recent Enhancements to Overflow," AIAA Paper 97-0644, January 1997.

¹¹Rogers, S. E., Roth, K., Nash, S. M., Baker, M. D., Slotnick, J. P., Whitlock, M., and Cao, H. V., "Advances in Overset CFD Processes Applied to Subsonic High-Lift Aircraft," AIAA Paper 2000-4216, August, 2000.

¹²Chan, W. M., "The Overgrid Interface for Computational Simulations on Overset Grids," AIAA Paper 2002-3188, June 2002.

¹³Suhs, N. E., Rogers, S. E., and Dietz, W. E. "PEGASUS 5: An Automated Pre-processor for Overset-Grid CFD," *AIAA Journal*, Vol. 41, No. 6, June 2003, pp. 1037-1045.

¹⁴Pulliam, T. H., and Chaussee, D. S., "A Diagonal Form of an Implicit Approximate-Factorization Algorithm," *Journal of Computational Physics*, Vol. 39, No. 2, 1981, pp. 347-363.

¹⁵Spalart, P. R., and Allmaras, S. R., "A One-Equation Turbulence Model for Aerodynamic Flows," AIAA Paper 92-0439, January 1992.

¹⁶Olsen, M. E., and Prabhu, D. K., "Application of Overflow to Hypersonic Perfect Gas Flowfields," AIAA Paper 2001-2664, June 2001.

¹⁷Jespersen, D. J., "Parallelism and Overflow," NAS Technical Report NAS-98-013, October 1998. <http://www.nas.nasa.gov/Pubs/TechReports/NASreports/NAS-98-013/>

¹⁸Taft, J. R., "Multi-Level Parallelism, "A Simple Highly Scalable Approach to Parallelism for CFD," HPCCP/CAS Workshop Proceedings, (C. Schulbach, ed.), 1998.

¹⁹Pamadi, B. N., Covell, P. F., Murphy, K. J., Borderlon Jr, W. J., and Frost., A. L., "Aerodynamic Characteristics of Langley Glide Back Booster", to be presented at the AIAA Aerosciences Meeting, Reno, Nevada, January 2004.

²⁰Butland, J., and Fritsch, F.N., "A Method for Constructing Local Monotone Piecewise Cubic Interpolants," *SIAM Journal on Scientific and Statistical Computing*, Vol. 5, No. 2, June 1984, pp. 300-304.